JACS
JOURNAL OF THE AMERICAN CHEMICAL SOCIETY
Article
pubs.acs.org/JACS

Confinement of Single Polysilane Chains in Coordination Nanospaces

Takashi Kitao,[†] Silvia Bracco,[‡] Angiolina Comotti,[‡] Piero Sozzani,[‡] Masanobu Naito,[§] Shu Seki,[∥] Takashi Uemura,*[,†,⊥] and Susumu Kitagawa*[,†,#]

[†]Department of Synthetic Chemistry and Biological Chemistry, Graduate School of Engineering, Kyoto University, Katsura, Nishikyo-ku, Kyoto 615-8510, Japan

[‡]Department of Materials Science, University of Milano Bicocca, Via R. Cozzi 55, 20125 Milan, Italy

[§]National Institute for Materials Science (NIMS), 1-1 Namiki, Tsukuba, Ibaraki 305-044, Japan

[∥]Department of Applied Chemistry, Graduate School of Engineering, Osaka University, 2-1 Yamadaoka, Suita, Osaka 565-0871, Japan

[⊥]CREST, Japan Science and Technology Agency (JST), 4-1-8 Honcho, Kawaguchi, Saitama 332-0012, Japan

[#]Institute for Integrated Cell-Material Sciences (WPI-iCeMS), Kyoto University, Yoshida, Sakyo-ku, Kyoto 606-8501, Japan

Supporting Information

ABSTRACT: Understanding the intrinsic properties of single conducting polymer chains is of interest, largely for their applications in molecular devices. In this study, we report the accommodation of single polysilane chains with hole-transporting ability in porous coordination polymers (PCPs), $[Al(OH)(L)]_n$ (**1a**; L = 2,6-naphthalenedicarboxylate, channel size = 8.5 × 8.5 Å^2, **1b**; L = 4,4′-biphenyldicarboxylate, channel size = 11.1 × 11.1 Å^2). Interestingly, the isolation of single polysilane chains increased the values of carrier mobility in comparison with that in the bulk state due to the elimination of the slow interchain hole hopping. Moreover, even when the chains are isolated one another, the main chain conformation of polysilane could be controlled by changing the pore environment of PCPs, as evidenced by Raman spectroscopy, solid-state NMR measurements, and molecular dynamics simulation. Hence, we succeeded in varying the conducting property of single polysilane chains. Additionally, polysilanes have a drawback, photodegradation under ultraviolet light, which should be overcome for the application of polysilanes. It is noteworthy that the accommodation of polysilane in the nanopores did not exhibit photodegradation. These results highlight that PCP−polysilane hybrids are promising candidates for further use in the field of molecular electronics.

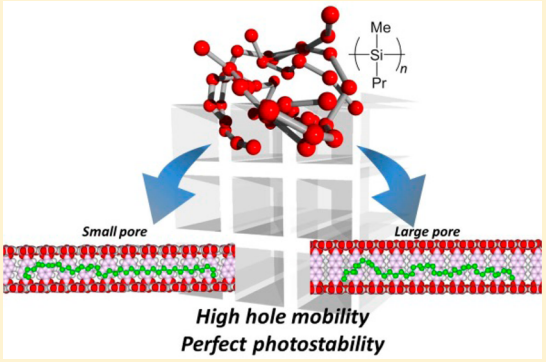

INTRODUCTION

Molecular devices will play a crucial role in the future for the growing interest of device miniaturization with the final goal of saving energy and space.[1−3] Conducting polymers can be expected to serve as molecular wires connecting organic molecules and electrodes; therefore, many attempts have been made to elucidate the properties of single conducting polymer chains.[4−6] Confinement of polymer chains in porous materials is a feasible method to isolate single polymer chains, permitting the study of their properties, such as conductivity and fluorescence of macromolecules in nanochannels of zeolites, mesoporous silicas, and organic crystalline hosts.[7−16] Indeed, this approach can prevent the entanglement and conformational disorder occurring in bulk polymers.[17,18] For future applications of such chemical entities in molecular-scale devices, there is a need to understand confinement effects that affect the properties of the individual chains.[19] As a consequence of the isolated chain state, the properties of the polymer might be radically affected by the environment surrounding the macromolecules: in fact, the size, shape, and surface functionality of the restricted spaces can deeply modulate the conformational and electronic structures of the polymers. In this regard, the preparation of properly engineered nanochannels with controlled pore structures is an essential prerequisite because they can offer opportunities to study confinement effects on single polymer chains in rationally designed pores.

For this purpose, we employed porous coordination polymers (PCPs) or metal−organic frameworks (MOFs), prepared by the self-assembly of metal ions and functional organic ligands,[20−22] which offer a wide range of applications, such as gas separation, heterogeneous catalysis, and sensing.[23−27] The advantages of PCPs are controllable channel size through the precise choice of organic ligands, metal ions, and synthesis conditions. Compared with the conventional porous materials, these intriguing features of PCPs allow us to achieve precise molecular assemblies in the nanochannels, which are of key importance for elucidating the properties of the confined

Received: March 2, 2015
Published: April 2, 2015

DOI: 10.1021/jacs.5b02215
J. Am. Chem. Soc. 2015, 137, 5231−5238

materials, such as phase transitions, dynamics, and ion mobility.[19,28,29]

Herein, we report the incorporation of polysilane into the nanochannels of PCPs as individual chains. Polysilanes exhibit unique optical and electrical properties, such as backbone electronic transition with UV−vis absorption, high quantum yield of fluorescence, and high mobility of charge carriers,[30−32] which are attributed to delocalization of σ-electrons along the main chain. The conformation of the polymer chain, which is sensitive to temperature (thermochromism) and to solvent (solvatochromism), strongly influences the σ-conjugation system.[33] However, the σ-conjugation of polysilane becomes inefficient under UV exposure because of photodegradation. Silyl radicals and silylenes were generated by the cleavage of the Si−Si bond using UV irradiation.[34] These species are unstable and react with oxygen molecules immediately to form siloxane and silanol structures, which causes a reduction in conjugation length and the consequent decrease of fluorescence quantum yield and carrier mobility. Therefore, improvement in photostability is highly desirable for light-emitting devices and solar cells.[35]

There have been only a few attempts to isolate polysilane chains, for example, by fixing the polymer chain-end to a solid surface or embedding polysilane into a silica-based materials.[36,37] However, the confinement and manipulation of single polysilane chains at the nanometric level has never been achieved so far. Here we fabricated host−guest adducts by inclusion of polymethylpropylsilane (PMPrS) in the nanochannels of two porous coordination polymers with distinct channel sizes (Figure 1). The PCPs of choices exhibited the general chemical formula $[Al(OH)(L)]_n$ in which the ligand (L) corresponds to 2,6-naphthalenedicarboxylate (DUT-4, denoted as **1a**) and 4,4′-biphenyldicarboxylate (DUT-5, denoted as **1b**) (Figure 1a, 1b). The channels with cross sections of 8.5 × 8.5 Å^2 and 11.1 × 11.1 Å^2, respectively, can accommodate individual polymer chains and precisely modulate their conformational properties. Moreover, the alternation of **1a** and **1b** enabled changing the conduction property of single polysilane chains. Indeed, the isolated polymer chains exhibited higher values of charge carrier mobility than that of the bulk state. Additionally, photodegradation phenomena of the polymer can be avoided by the host crystal structure, which acted as a protective shell for the macromolecules.

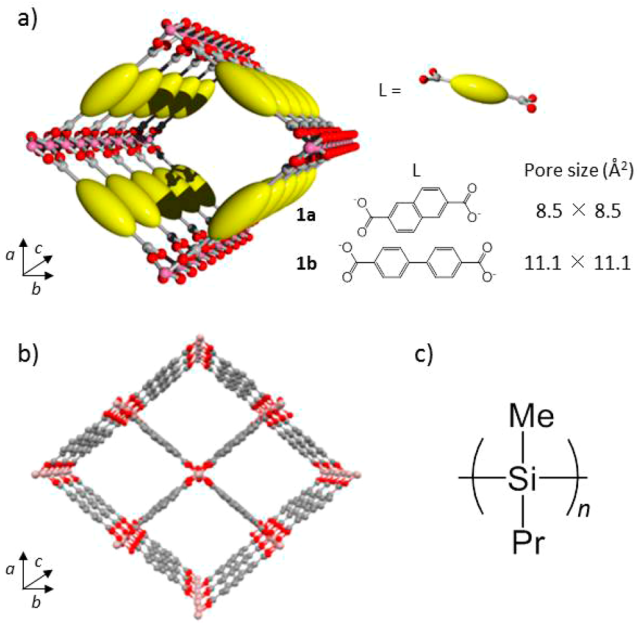

Figure 1. (a) Schematic image for nanochannel structures of PCP hosts. $[Al(OH)L]_n$ (Al, pink; O, red; C, gray; **1a**, L = 2,6-naphthalenedicarboxylate; **1b**, L = 4,4′-biphenyldicarboxylate). (b) X-ray structures of **1a** (Al, pink; O, red; C, gray). Hydrogen atoms are omitted for clarity. (c) Molecular structure of polymethylpropylsilane.

EXPERIMENTAL SECTION

Materials. All of the reagents and chemicals used were obtained from commercial sources, unless otherwise noted. **1** was prepared according to previously described methods.[38]

Synthesis of PMPrS. PMPrS was prepared using the Wurtz-type condensation reaction of dichloromethylpropylsilane (20 mmol) with sodium in toluene (14 mL) at 120 °C for 2 h in the presence of chlorotrimethylsilane (10 mmol) as a terminator, and then isolated by fractional precipitation with careful successive additions of 2-propanol (5 mL) and methanol (5 mL) to eliminate the higher molecular weight fraction of the bimodal distribution. The insoluble PMPrS fraction after the addition of methanol was dried in a vacuum (yield: 19%). Gel-permeation chromatography (GPC) measurement of the resultant PMPrS showed a number-average molecular weight (M_n) of 3600 with respect to a polystyrene standard.

Introduction of PMPrS into 1. The host−guest composites of **1**⊃PMPrS were prepared by direct encapsulation of PMPrS into host matrices. The inclusion ratio of PMPrS to **1** was adjusted not to exceed the completely filled amounts in the nanochannels. The general incorporation procedure was as follows. Compound **1** (150 mg) was dried by evacuation at 150 °C for 5 h. Subsequently, the host powder was immersed in hexane solution (1 mL) of PMPrS (64 mg) at room temperature. To incorporate PMPrS into the nanochannels, hexane was completely removed by evacuation at an elevated temperature of 120 °C for 12 h to obtain powdery composites (211 mg).

Photoirradiation of Bulk PMPrS and 1⊃PMPrS. UV light was irradiated upon **1**⊃PMPrS and bulk PMPrS under air atmosphere with a 500 W ultrahigh-pressure mercury lamp (300−400 nm) for 24 h at room temperature.

Extraction of PMPrS. **1**⊃PMPrS was stirred for 0.5 h in 0.05 M aqueous solution of sodium ethylenediaminetetraacetate (Na_4-EDTA) to decompose **1**; subsequently, hexane was used to extract PMPrS from an aqueous solution. The isolated PMPrS was washed with water and dried under a reduced pressure at room temperature.

Measurement. X-ray powder diffraction (XRPD) data were collected on a Rigaku RINT 2000 Ultima diffractometer with Cu Kα radiation. The adsorption isotherms of nitrogen at 77 K were measured by BELSORP-mini equipment. Before the adsorption measurements, the sample was treated under reduced pressure (<10^{-2} Pa) at 373 K for 5 h. Particle size distributions of dry powder samples were measured using a HORIBA Partica LA-950 laser diffraction particle size analyzer. Microscopic Raman spectroscopy was carried out using a LabRAM HR-800 spectrometer (HORIBA Jobin Yvon Ltd.) at temperatures in the range 300−353 K using an LK-600 hot stage (Linkam). A 785 nm semiconductor laser was used as the excitation source. Differential scanning calorimetry (DSC) was carried out with Seiko Instruments DSC 6220 under N2 atm. The scanning electron microscopy (SEM) images were collected by using a Hitachi S-3000N SEM system operated at an accelerating voltage of 20 kV. Samples were placed on a conducting carbon tape attached by SEM grid, and then coated with platinum. Gel permeation chromatograph measurement on the PMPrS was performed in $CHCl_3$ at 40 °C on three linear-type polystyrene gel columns (Shodex K-805L) that were connected to a Jasco PU-980 precision pump, a Jasco RI-930 refractive index detector, and a Jasco UV-970 UV−vis detector set at 256 nm. UV−vis spectra were recorded on a JASCO V-670 spectrometer. The solid-state NMR spectra were run at 75.5 MHz for ^{13}C and at 59.6 MHz for ^{29}Si on a Bruker Avance 300 instrument operating at a static

DOI: 10.1021/jacs.5b02215
J. Am. Chem. Soc. 2015, 137, 5231−5238

field of 7.04 T equipped with high-power amplifiers (1 kW) and a 4 mm double resonance MAS probe. The samples were spun at a spinning speed of 15 kHz, and ramped-amplitude cross-polarization (RAMP−CP) transfer of magnetization was applied. The 90° pulse for protons was 2.9 μs (86 kHz). ^{13}C and ^{29}Si cross-polarization (CP) magic angle spinning (MAS) experiments were performed using a recycle delay of 6 s and a contact time of 2 and 8 ms, respectively. Quantitative fully relaxed ^{13}C and ^{29}Si single-pulse excitation (SPE) experiments with dipolar decoupling from hydrogen were run using a recycle delay of 100 s. Phase-modulated Lee−Goldburg (PMLG) heteronuclear ^{1}H−^{13}C and ^{1}H−^{29}Si correlation (HETCOR) experiments combined with fast MAS allowed the recording of 2-D spectra with high resolution both in the hydrogen and rare-nuclei dimensions. PMLG ^{1}H−^{13}C and ^{1}H−^{29}Si HETCOR spectra were run with an LG period of 18.9 μs. Quadrature detection in t_1 was achieved using the time proportional phase increments (TPPI) method. Efficient transfer of magnetization to the carbon nuclei was performed applying a RAMP−CP sequence. CP times from 2 to 8 ms were applied. Carbon and silicon signals were acquired during t_2 under proton decoupling applying a two-pulse phase modulation (TPPM) scheme. Quantitative ^{1}H MAS NMR measurements were performed with a Bruker Avance III 600 MHz instrument operating at 14.1 T, using a recycle delay of 20 s. A MAS Bruker probe head was used with 2.5 mm ZrO_2 rotors spinning at 33 kHz. 2-D ^{1}H double-quantum combined rotation and multiple pulse spectroscopy (2-D ^{1}H DQ CRAMPS) experiments were run at a MAS frequency of 13.6 kHz. The excitations and reconversion of DQ coherence (DQC) was achieved using the POST-C7 recoupling sequence, while windowed phase-modulated Lee−Goldburg decoupling sequences (*w*PMLG) were applied in t_1 and t_2.

Molecular Dynamics (MD) Simulations. MD simulations were performed using the Materials Studio Modeling v4.4 software package (Accelrys Inc., San Diego, CA, USA) using the Universal Force Field, as implemented in the Forcite module. The charges were dealt with by the charge equilibration method in this system. The initial structure of **1** was generated based on the X-ray crystal structure of **1**. The quench dynamics with the optimized structures were conducted at 493 K, and then, MD calculations were carried out at 293 K for 1000 ps under NVT conditions.

Time-Resolved Microwave Conductivity (TRMC) Measurements. Excitation was carried out using nanosecond laser pulses of a Nd:YAG laser (third harmonic generation, THG (355 nm) and FHG (266 nm) from Spectra Physics, INDI-HG, fwhm 3−5 ns). The photon density of the laser was set at 1.0×10^{16} photons/cm^2. The microwave frequency and power were set at ∼9.1 GHz and 3 mW, respectively, for the flash-photolysis (FP)−TRMC measurement, and the polycrystalline film of **1**⊃PMPrS in PMMA matrix fixed onto a quartz substrate was set at the electric field maximum in the microwave cavity. All of the above experiments were carried out at room temperature. Photoconductivity transients ($\Delta\sigma$) in the samples are given as a function of photocarrier generation yield (Φ) and the sum ($\Sigma\mu$) of the mobilities of positive (μ^+) and negative (μ^-) charge carriers as

$$\Delta\sigma = eN\Phi \sum \mu \qquad (1)$$

and the value of Φ was determined from the transient absorption spectroscopy (TAS) of the sample. The number of photons absorbed by the sample was estimated based on the power loss of incident laser pulses averaged over 128 shots. The other details of the setup of the FP−TRMC apparatus are described elsewhere.[4,39] An in situ TAS measurement assigned the conductivity kinetics to positive charge species and determined its concentration quantitatively. The THG and FHG laser pulses from the nanosecond laser were used as excitation light sources. The incident excitation photon densities in the present paper were set at 1.0×10^{16} photons/cm^2. The continuum white light from a Xe lamp was used as a monitor light source, and in situ spectroscopy of TAS and kinetics were carried out over the time and wavelength ranges of 12−32 μs and 380−440 nm, respectively. The value of Φ was determined based on the transient absorption observed at 400 nm attributed to radical cations with ε^+ of 3.8×10^4 mol^{-1} dm^3 cm^{-1}.[40] The monitoring white light continuum as well as emission from the polycrystalline **1**⊃PMPrS was passed to a grating unit (Hamamatsu, C5094) and scanned by a wide-dynamic-range streak camera (Hamamatsu, C7700). The streak image was collected via a CCD camera (Hamamatsu, C4742−98). To examine the value of Φ for bulk PMPrS, TRMC and TAS measurements were carried out in a PMMA matrix with *N*,*N*′-bis(2,5-di-*tert*-butylphenyl)-3,4,9,10-perylenedicarboximide (PDI, 10 wt %). The PDI is useful to estimate Φ through monitoring of the radical anions generated by photoinduced electron transfer.[41]

RESULTS AND DISCUSSION

Characterization of 1⊃PMPrS. PMPrS was prepared by a Wurtz-type condensation reaction using chlorotrimethylsilane as a terminator to obtain PMPrS with relatively low molecular weight (M_n = 3600, M_w/M_n = 1.64). Then, PMPrS was introduced into the nanochannels of **1** at an elevated temperature of 120 °C (above the melting temperature of neat PMPrS) via polymer melt processing, providing the nanocomposite **1**⊃PMPrS. Considering the channel size of **1** (**1a**: 8.5 × 8.5 Å^2; **1b**: 11.1 × 11.1 Å^2) and the lateral encumbrance of PMPrS (7.4 Å), a single-chain would be incorporated in each channel of **1**. The PMPrS mass fraction in the nanocomposites corresponded to 0.3: this value was optimized so that the amount of the polymer did not exceed the capacity of the nanochannels.

Formation of the resulting composites was confirmed by X-ray powder diffraction (XRPD). The diffraction pattern of **1**⊃PMPrS compounds did not contain any peaks ascribable to bulk PMPrS (Figure 2a). No change in the peak positions was observed after incorporation of PMPrS, indicating that the crystal structures of **1** were maintained on inclusion of PMPrS. The introduction of PMPrS into the nanochannels of **1** was

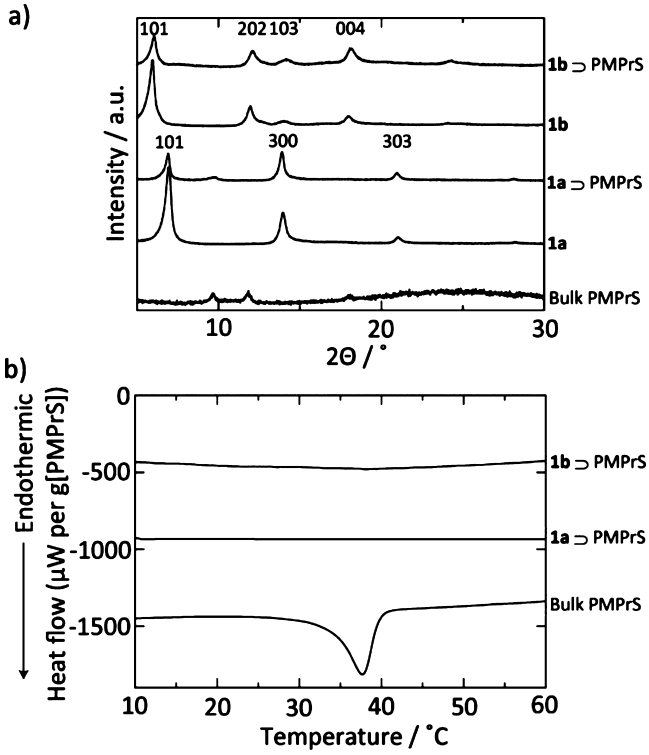

Figure 2. (a) XRPD patterns and (b) DSC heating curves of bulk PMPrS, **1**, and **1**⊃PMPrS. The heating rate of the measurements was 10 K min^{-1}.

DOI: 10.1021/jacs.5b02215
J. Am. Chem. Soc. 2015, 137, 5231−5238

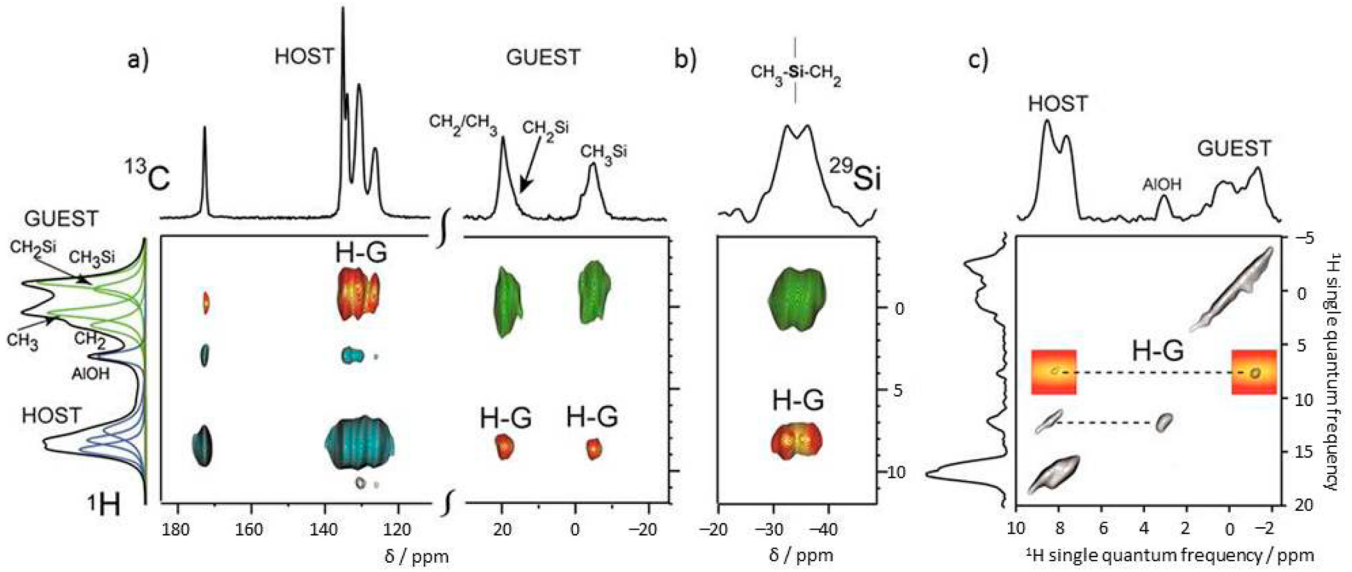

Figure 3. 2-D HETCOR NMR spectra of **1a**⊃PMPrS: (a), (b) ^{1}H−^{13}C and ^{1}H−^{29}Si spectra recorded by applying phase-modulated Lee−Goldburg decoupling and contact times of 2 and 8 ms, respectively. In the hydrogen domain, the 1-D ^{1}H MAS spectrum (600 MHz and 33 kHz spinning speed) is reported. In the carbon and silicon domains, the ^{13}C CP−MAS spectrum at 75.5 MHz and the ^{29}Si projection at 59.6 MHz are reported, respectively. Blue, green, and orange cross-signals correspond to host−host, guest−guest, and host−guest interactions, respectively. (c) 2-D ^{1}H−^{1}H DQ CRAMPS NMR spectrum of **1a**⊃PMPrS (600 MHz and 13.6 kHz spinning speed). Host−guest correlations are indicated in orange.

evident from the change in the relative peak intensities because of the different electron density distribution when the polymer is confined in the channels.[19] The DSC scan for the neat PMPrS sample presented an endothermic peak at 37 °C as the melting temperature of PMPrS (Figure 2b). In contrast, no transitions were detected in the nanocomposites, suggesting no excess PMPrS existed outside **1** (Figure 2b). For comparison, samples with an excess polymer (polymer mass fraction of 0.4) showed a small endothermic peak, corresponding to the melting of excess PMPS lying outside the nanochannels (Figure S1, Supporting Information). The nitrogen adsorption measurement of **1**⊃PMPrS showed the drastic decrease in the amount of adsorption compared with those of the pristine empty hosts, verifying the presence of PMPrS within the nanochannels (Figure S2). In addition, SEM images showed that the crystal size and morphology of the host compounds did not change after introduction of PMPrS, which is consistent with the analysis of particle size distribution by laser light diffraction (Figures S3 and S4). This is a clear indication that no excess polymer is deposited over the crystals and the host crystal structure is fully retained after polymer migration into the channels.

Independent information concerning the composition of the nanostructured materials was obtained from high resolution ^{1}H MAS NMR spectra recorded at 600 MHz (Figure S5). The spectra exhibited the characteristic signals of polysilane and host matrix and the quantitative evaluation of the peak integrals indicates that the molar ratio between the host ligand and the monomer unit of the polymer was 1:1.1 and 1:1.3 for **1a**⊃PMPrS and **1b**⊃PMPrS, respectively. This result ensures that the polymer does not exceed the amount necessary to fill the channels.

Multinuclear 2-D NMR is a powerful method to provide information about the components in a complex system and especially in host−guest systems, in which the two constituents are intimately interacting. Notably, the 2-D ^{1}H−^{13}C HETCOR NMR spectrum of **1a**⊃PMPrS (Figure 3a), performed under Lee−Goldburg homonuclear decoupling and 2 ms CP time, highlighted not only the intramolecular correlations of the host and the guest separately, but exhibited cross-peaks associated with the intermolecular host−guest interactions that occurred through dipole−dipole interactions at short distances of less than 5 Å.[42] In Figure 3a, the intense cross correlations that arise from the aromatic hydrogens of the host ligand (δ_H = 8.1 ppm) to the carbon nuclei of guest PMPrS (δ_C = 20.1 and −4.9 ppm) and from guest hydrogens (δ_H = −1 ppm) to the host matrix (δ_C = 130−135 ppm) are highlighted in orange. The 2-D ^{1}H−^{29}Si HETCOR spectrum also revealed the through-space host−guest interactions; in fact, intense cross correlations between the host aromatic hydrogens and silicon atoms of the silicon backbone of the guest polymer were observed (Figure 3b). Moreover, the extended host−guest interface was strikingly corroborated by the solid-state 2-D ^{1}H−^{1}H DQ CRAMPS NMR spectrum, performed at 600 MHz ^{1}H Larmor frequency and applying *w*-PMLG decoupling in both dimensions to achieve high resolution in the proton domain.[43−46] This NMR technique brings to light a unique observation of intermolecular host−guest relationships across the extended interfaces, exploiting the ^{1}H−^{1}H dipolar coupling to probe through-space proximities between host and guest protons. In the 2-D ^{1}H−^{1}H spectrum of Figure 3c, the correlations between host and guest hydrogens emerge, providing a direct observation of the polymer chains included in the host nanochannels.

Similarly, the 2-D ^{1}H−^{13}C and ^{1}H−^{29}Si 2-D NMR spectra of **1b**⊃PMPrS composite (Figure S6) clearly underlined the close proximity of the polymer to the matrix and thus the accommodation of guest polymer chains in the host pores, although in the 2-D ^{1}H−^{13}C NMR spectrum, intense cross-peaks were detected only at longer contact times (e.g., 5 ms). These results demonstrate that the confined polymer chains are located at longer distances with respect to the host ligands in matrix **1b**, while the polymer chains sit at shorter distances in **1a** because they are encapsulated in narrower nanochannels.

DOI: 10.1021/jacs.5b02215
J. Am. Chem. Soc. 2015, 137, 5231−5238

Conformation of PMPrS in 1. The molecular conformation of PMPrS encapsulated in **1** was investigated using Raman spectroscopy (Figure 4). The intensity of the peak corresponding to the symmetric stretching vibrations ν(Si−C) at ca. 670 cm^{-1} strongly depends on the main chain conformation.[47] The relative intensity of this peak increases with increasing the amount of s-trans conformation. In our materials, the intensity of the ν(Si−C) peak of **1a**⊃PMPrS was higher than that of **1b**⊃PMPrS, indicating that PMPrS chains preferred to form a linear structure with increasing s-trans conformation in the smaller channels of **1a**. At room temperature, the intensity of the ν(Si−C) peak of bulk PMPrS is similar to that of **1a**⊃PMPrS. This is because bulk PMPrS includes crystalline s-trans conformation.[48] On heating the bulk PMPrS from room temperature to 80 °C, the intensity of the peak underwent a large change, which showed the transformation from solid to liquid states accompanied by a large conformational change in the PMPrS chains.[47] However, it was striking that the intensity of PMPrS in **1a** was almost unchanged at the same temperature of 80 °C (Figure 4). A stretched conformation of PMPrS resulted from the confinement effect of **1a**, in which the PMPrS chains were forced to form an extended linear structure in the narrow 1-D channels.[49]

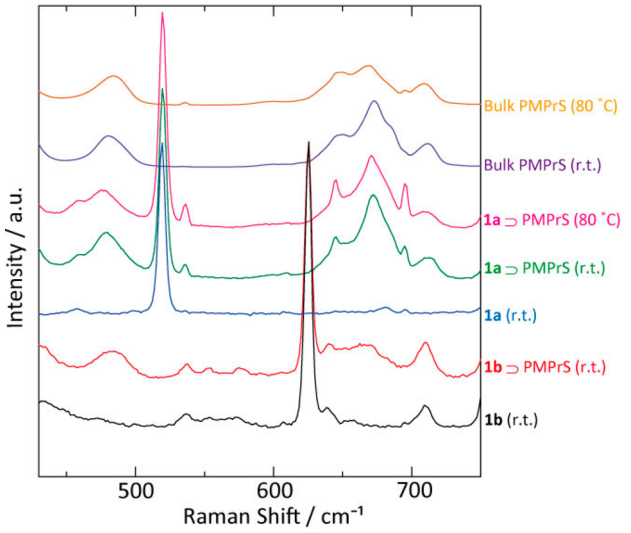

Figure 4. Variable temperature Raman spectra of **1**, **1**⊃PMPrS, and bulk PMPrS.

Fully relaxed ^{29}Si MAS NMR experiments detected the polymer main-chain nuclei as two signals resonating at about δ_{Si} = −32 and −36 ppm (Figure 5a, 5b): the downfield signal prevails when the polymer is confined to the narrow channel of host **1a**, whereas the upfield signal prevails for the polymer in the wider cavities of host **1b**. The signal multiplicity cannot be due to structural defects or stereochemical sequences because a single narrow peak was exhibited by the bulk polymer in solution. Instead, the backbone conformations adopted by the polymer included in the two distinct-size pores are the origin of the ^{29}Si chemical shift change. Specifically, the trans conformation of the main chain implies two gauche arrangements of C_1 (C_1 = CH_3 or CH_2) carbon atoms of the side groups with respect to the observed Si nucleus (Figure 5a), whereas a deviation of the main chain away from the trans conformation of about 30° rotates the Si−Si−Si−C_1 dihedral angle toward an eclipsed arrangement (see Figure 5a), as described in the literature for polysilane conformers in polymorphic phases.[50] The quasi-eclipsed conformation produces a remarkable shielding effect of about 4 ppm in the ^{29}Si spectrum and is at the origin of the signal at δ_{Si} = −36 ppm. The stretched trans conformation prevails in the narrow channel, which induced severe lateral confinement squeezing the polymer chain, while the extra room available in the wider channels allows for the development of cumbersome main-chain conformations that explore frequent arrangements deviating from trans. Such a fine control of the polymer conformations and a sensible NMR-resonance shift were rarely obtained by inclusion in nanochannels or by mechanical stretching.[51−54]

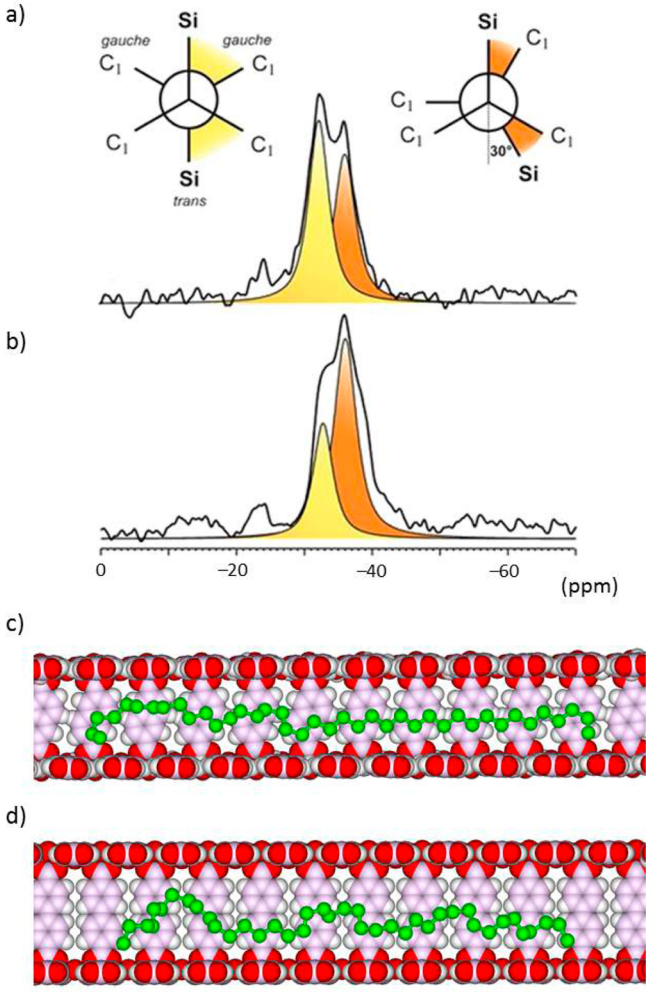

Figure 5. ^{29}Si MAS NMR spectra of **1a**⊃PMPrS (a) and **1b**⊃PMPrS (b) recorded with a recycle delay of 100 s. The Newman projections viewed along the main-chain Si−Si bond are associated with the downfield (yellow) and upfield (orange) signals. Conformational arrangement of the included polymer as derived by MD simulation: (c) in the narrow channel of host **1a** and (d) in the wide channel of host **1b**. Substituents of PMPrS are omitted for clarity. (Si, light green; O, red; C, light pink; H, white.).

Furthermore, the conformation of PMPrS chains confined in the nanochannels was studied theoretically using the molecular dynamics (MD) method (Figure 5c, 5d). In MD simulations, PMPrS chains in **1a** formed an extended linear structure in the narrow 1-D channels in a single-chain manner; in contrast, those in **1b** formed a disordered chain conformation, which is consistent with the results of ^{29}Si MAS NMR and the Raman

DOI: 10.1021/jacs.5b02215
J. Am. Chem. Soc. 2015, 137, 5231−5238

spectroscopy measurements. The overall characterizations of **1**⊃PMPS compounds clearly indicated that single polysilane chains are included into the nanopores and rare control of the conformation of polysilane chains by tuning the pore size of PCPs was achieved.

Charge Carrier Mobility of PMPrS in 1. To study the carrier mobility of single polysilane chains, we performed a transient photoconductivity ($\phi\Sigma\mu$) measurement of bulk PMPrS and **1**⊃PMPrS using FP−TRMC measurements, in which ϕ and $\Sigma\mu$ are the charge carrier generation yield and the sum of the charge carrier mobilities, respectively.[39,55,56] The values of ϕ were derived from TAS measurements. To facilitate the charge carrier generation of bulk PMPrS, FP−TRMC and TAS measurements were carried out in polymer film blended with PDI.[57] **1**⊃PMPrS and bulk PMPrS displayed a clear conductivity signal (Figures 6 and S7). Interestingly, the

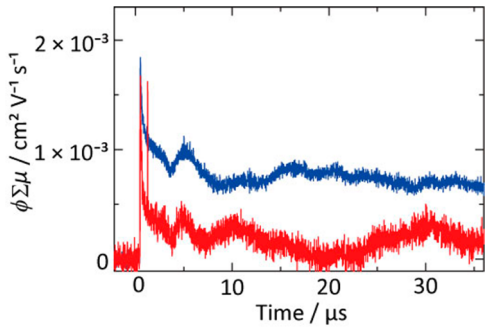

Figure 6. Transient conductivities observed for **1a**⊃PMPrS (blue) and **1b**⊃PMPrS (red). The transients were recorded under 355 nm laser pulse excitation at 1.0×10^{16} photons cm^{-2}.

introduction of single polysilane chains led to the increase in the carrier mobility, which was more than one order magnitude higher than that in the bulk state (**1a**⊃PMPrS: $\mu = 3.0 \times 10^{-2}$ cm^2 V^{-1} s^{-1}, **1b**⊃PMPrS: 1.5×10^{-2} cm^2 V^{-1} s^{-1}, bulk PMPrS: 1.0×10^{-3} cm^2 V^{-1} s^{-1}). Host **1** did not give any transient photoconductivity signals, confirming that the high carrier mobility in **1**⊃PMPrS resulted from the single polysilane chains accommodated in **1** (Figure S8). In the solid state, the charge transport takes place through not only intrachain but also interchain hopping.[29,58] The higher carrier mobility of PMPrS in **1** should originate from the elimination of slower interchain hopping because of the single-chain manner.

Single polysilane chains in **1a** and **1b** represented the different conformations, which would affect its carrier transport property because the dominant process of charge carrier transport in polysilanes is the hopping of holes between domain-like subunits long the Si chain whose size is influenced by the backbone conformation.[59,60] In our system, the carrier mobility of PMPrS chains in **1a** was higher, probably because of the more linearly extended conformation of PMPrS in **1a** than that in **1b** (Figure 6). This result indicated that properties of polysilanes can be modulated even in a single-chain manner. Here, in case of the confinement of a charge carrier in a conjugated backbone unit with the persistence length, the following equation gives an estimate of the local dislocation Δx of charge carriers induced by the electric field of the microwave in alternating current mode with the frequency f, where k_B and e are Boltzmann's constant and an elementary charger, respectively.

$$q = \Delta x = \left(\mu \frac{k_B T}{fe}\right)^{1/2} \quad (2)$$

On the basis of the obtained values of local hole mobility along PMPrS backbone in the nanopores of **1a** and **1b**, the derived values of the dislocation were proved to be 0.88 and 1.53 nm, respectively. These values are longer than the persistence length of PMPrS reported as $q \sim 0.4$ nm, which suggested that the confinement of polymer chain is also an effective method for the enhancement of the carrier transport properties.[61]

UV Stability of PMPrS in 1. Stability to UV light of polysilanes is important for optoelectrical applications; however, polysilanes are sensitive to ultraviolet light.[62] UV irradiation induces the destruction of σ-conjugation resulting from the breaking of Si−Si bonds and the accompanying incorporation of oxygen into the silicon structures. After UV irradiation, the UV absorption spectrum of neat PMPrS underwent a drastic change. The peak intensity at 302 nm decreased because of the formation of the oxygen adducts. In addition, the molecular weight of PMPrS decreased after UV irradiation for 24 h, which suggested that the silylene extrusion also occurred to shorten the chain length (Figure S9).[63] The photostability of PMPrS constrained in the pores was investigated by exposing **1**⊃PMPrS to UV light. PMPrS was extracted with hexane after dissolving **1** in 0.05 M Na_4-EDTA solution for the UV measurement. In highly contrast to the case of bulk PMPrS, the UV spectra of PMPrS isolated from **1**⊃PMPrS showed that the peak at 302 nm was unchanged, indicating the complete maintenance of σ-conjugation system (Figure 7). Moreover, it was notable that there was no change

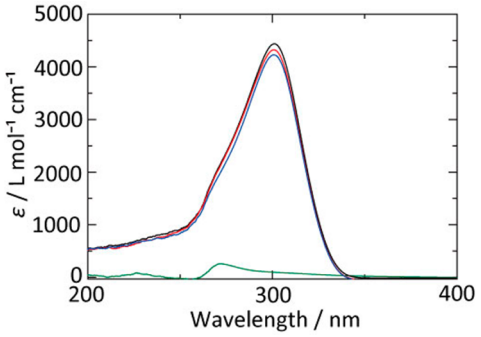

Figure 7. UV spectra of bulk PMPrS (black), bulk PMPrS after UV irradiation (green), and PMPrS extracted from **1a**⊃PMPrS (red) and **1b**⊃PMPrS (blue) after UV irradiation. ε: molar absorption coefficient per Si unit. Solvent: hexane.

in molecular weight of PMPrS after UV irradiation (Figure S9). These results indicate that the Si−Si bond was maintained. The increased photostability makes the PCP−polymer hybrids good candidates for improving the performance of optoelectronic devices.

To investigate the reason for the enhancement of the photostability of PMPrS in the nanopores, a TAS measurement was carried out on **1a**⊃PMPrS after 355 nm laser pulse exposure. In the transient absorption spectrum, a broad peak could be observed around 450 nm, probably because of the generation of silylene or silyl radicals (Figure S10).[64] These are highly unstable species that readily react with alcohols and even atmospheric oxygen.[33,34,64] In fact, this peak disappeared after the addition of methanol as a quencher of these species (Figure

DOI: 10.1021/jacs.5b02215
J. Am. Chem. Soc. 2015, 137, 5231−5238

S10). However, the UV spectra of **1**⊃PMPrS showed that the Si−Si bond in PMPrS was retained even after UV irradiation, suggesting that polysilane chains in **1** are not susceptible to attack by atmospheric oxygen, compared with bulk polysilane.[14] In fact, **1**⊃PMPrS showed a negligible amount of oxygen adsorption at 298 K, where the ratio of adsorbed oxygen to **1**⊃PMPrS was $<10^{-5}$ wt %. From the obtained results, we could deduce that transient species, generated by cleavage of the Si−Si bond after UV irradiation, were stabilized in the nanopores because of protection from oxygen molecules, which led to recombination of the Si−Si bond. Also, the suppression of the silylene extrusion in the nanopores due to the steric hindrance would attribute to maintain the chain length. Therefore, the confinement of polymer chains in the pores could be considered to be an important key for the enhancement of photostability.

CONCLUSIONS

Understanding the properties of single polymer chains is important because of their potential application as molecular-based devices. In this work, we have demonstrated a facile methodology for elucidating the confinement effect on the properties of single polysilane chains with conductivity by using PCPs as a host. Single polysilane chains confined in the nanospaces showed higher values of charge carrier mobility than that of bulk polysilane because of elimination of the slow interchain carrier hopping. In addition, the conformation of the polysilane chains could be controlled, depending on the pore size, which allowed to manipulate precisely the carrier transport property of polysilanes even in the single-chain manner. Polysilane confined in the PCPs exhibited highly improved photostability compared with neat polysilane. These results illustrate that the nanoconfinement of polymer chains is a key strategy for improving the properties. We believe that these findings will contribute not only to significant progress in understanding intrinsic properties of conductive polymers but also to the preparation of a variety of advanced nanocomposite materials based on PCPs and functional polymers.

ASSOCIATED CONTENT

Supporting Information

DSC, adsorption isotherms, SEM, particle size distribution, NMR spectra, TRMC measurements, GPC, and TAS spectra. This material is available free of charge via the Internet at http://pubs.acs.org.

AUTHOR INFORMATION

Corresponding Authors

*uemura@sbchem.kyoto-u.ac.jp
*kitagawa@icems.kyoto-u.ac.jp

Notes

The authors declare no competing financial interest.

ACKNOWLEDGMENTS

This work was supported by the JST, CREST program, and a Grant-in-Aid for Scientific Research on Innovative Area "New Polymeric Materials Based on Element-Blocks (No. 2401)" from the Ministry of Education, Culture, Sports, Science and Technology, Government of Japan. A.C. would like to thank PRIN 2011 and Fondazione Cariplo 2012 for financial support.

REFERENCES

(1) Aviram, A.; Ratner, M. A. *Chem. Phys. Lett.* **1974**, *29*, 277−283.
(2) Joachim, C.; Gimzewski, J. K.; Aviram, A. *Nature* **2000**, *408*, 541−548.
(3) Metzger, R. M. *Chem. Rev.* **2003**, *103*, 3803−3834.
(4) Grozema, F. C.; Siebbeles, L. D. A.; Warman, J. M.; Seki, S.; Tagawa, S.; Scherf, U. *Adv. Mater.* **2002**, *14*, 228−231.
(5) Okawa, Y.; Aono, M. *Nature* **2001**, *409*, 683−684.
(6) Sakaguchi, H.; Matsumura, H.; Gong, H.; Adouelwafa, A. *Science* **2005**, *310*, 1002−1006.
(7) Sozzani, P.; Comotti, A.; Bracco, S.; Simonutti, R. *Angew. Chem., Int. Ed.* **2004**, *43*, 2792−2797.
(8) Nguyen, T. Q.; Wu, J. J.; Doan, V.; Schwartz, B. J.; Tolbert, S. H. *Science* **2000**, *288*, 652−656.
(9) Comotti, A.; Bracco, S.; Mauri, M.; Mottadelli, S.; Ben, T.; Qiu, S. L.; Sozzani, P. *Angew. Chem., Int. Ed.* **2012**, *51*, 10136−10140.
(10) Uemura, T.; Horike, S.; Kitagawa, K.; Mizuno, M.; Endo, K.; Bracco, S.; Comotti, A.; Sozzani, P.; Nagaoka, M.; Kitagawa, S. *J. Am. Chem. Soc.* **2008**, *130*, 6781−6788.
(11) Sozzani, P.; Bracco, S.; Comotti, A.; Valsesia, P.; Simonutti, R.; Sakamoto, Y.; Terasaki, O. *Nat. Mater.* **2006**, *5*, 545−551.
(12) Wu, C. G.; Bein, T. *Science* **1994**, *264*, 1757−1759.
(13) Esnouf, S.; Beuneu, F.; Enzei, P.; Bein, T. *Phys. Rev. B: Condens. Matter Mater. Phys.* **1997**, *56*, 12899−12904.
(14) Cucinotta, F.; Carniato, F.; Paul, G.; Bracco, S.; Bisio, C.; Caldarelli, S.; Marchese, L. *Chem. Mater.* **2011**, *23*, 2803−2809.
(15) Gierschner, J.; Lüer, L.; Oelkrug, D.; Musluoğlu, E.; Behnisch, B.; Hanack, M. *Adv. Mater.* **2000**, *12*, 757−761.
(16) Cardin, D. *Adv. Mater.* **2002**, *14*, 553−563.
(17) Bracco, S.; Comotti, A.; Ferretti, L.; Sozzani, P. *J. Am. Chem. Soc.* **2011**, *133*, 8982−8994.
(18) Sozzani, P.; Bracco, S.; Comotti, A.; Simonutti, R. *Adv. Polym. Sci.* **2005**, *181*, 153−177.
(19) Uemura, T.; Yanai, N.; Watanabe, S.; Tanaka, H.; Numaguchi, R.; Miyahara, M.; Ohta, Y.; Nagaoka, M.; Kitagawa, S. *Nat. Commun.* **2010**, *1*, 83.
(20) Yaghi, O. M.; O'Keeffe, M.; Ockwig, N. W.; Chae, H. K.; Eddaoudi, M.; Kim, J. *Nature* **2003**, *423*, 705−714.
(21) Férey, G.; Serre, C. *Chem. Soc. Rev.* **2009**, *38*, 1380−1399.
(22) Kitagawa, S.; Kitaura, R.; Noro, S.-i. *Angew. Chem., Int. Ed.* **2004**, *43*, 2334−2375.
(23) Sumida, K.; Rogow, D. L.; Mason, J. A.; McDonald, T. M.; Bloch, E. D.; Herm, Z. R.; Bae, T.-H.; Long, J. R. *Chem. Rev.* **2012**, *112*, 724−781.
(24) Wu, C.-D.; Hu, A.; Zhang, L.; Lin, W. *J. Am. Chem. Soc.* **2005**, *127*, 8940−8941.
(25) Kreno, J. E.; Leorg, K.; Farha, O. K.; Allendorf, M.; Van Duyne, R. P.; Hupp, J. T. *Chem. Rev.* **2012**, *112*, 1105−1125.
(26) Zacher, D.; Shekhah, O.; Wöll, C.; Fischer, R. A. *Chem. Soc. Rev.* **2009**, *38*, 1418−1429.
(27) Li, J. R.; Kuppler, R. J.; Zhou, H.-C. *Chem. Soc. Rev.* **2009**, *38*, 1477−1504.
(28) Bureekaew, S.; Horike, S.; Higuchi, M.; Mizuno, M.; Kawamura, T.; Tanaka, D.; Yanai, N.; Kitagawa, S. *Nat. Mater.* **2009**, *8*, 831−836.
(29) Ueda, T.; Kurokawa, K.; Kawamura, Y.; Miyakubo, K.; Eguchi, T. *J. Phys. Chem. C* **2012**, *116*, 1012−1019.
(30) Fujiki, M. *J. Am. Chem. Soc.* **1996**, *118*, 7424−7425.
(31) Kepler, R. G.; Zeigler, J. M.; Harrah, L. A.; Kurtz, S. R. *Phys. Rev. B: Condens. Matter Mater. Phys.* **1987**, *35*, 2818−2822.
(32) Harrah, L. A.; Zeigler, J. M. *Macromolecules* **1987**, *20*, 601−608.
(33) Miller, R. D.; Michil, J. *Chem. Rev.* **1989**, *89*, 1359−1410.
(34) Trefonas, P. T., III; West, R.; Miller, R. D. *J. Am. Chem. Soc.* **1985**, *107*, 2737−2742.
(35) Kamata, N.; Terunuma, D.; Ishii, R.; Satoh, H.; Aihara, S.; Yaoita, Y.; Tonsyo, S. *J. Organomet. Chem.* **2003**, *685*, 235−242.
(36) Furukawa, K.; Ebata, K.; Matsumoto, N. *Appl. Phys. Lett.* **1999**, *75*, 781−783.
(37) Kobayashi, A.; Naito, H.; Matsuura, Y.; Matsukawa, K.; Inoue, H.; Kanemitsu, Y. *Synth. Met.* **2003**, *135*, 297−298.

DOI: 10.1021/jacs.5b02215
J. Am. Chem. Soc. 2015, 137, 5231−5238

(38) Senkovska, I.; Hoffmann, F.; Fröba, M.; Getzschmann, J.; Böhlmann, W.; Kaskel, S. *Microporous Mesoporous Mater.* **2009**, *122*, 93−98.
(39) Saeki, A.; Seki, S.; Sunagawa, T.; Ushida, K.; Tagawa, S. *Philos. Mag.* **2006**, *86*, 1261−1276.
(40) Seki, S.; Koizumi, Y.; Kawaguchi, T.; Habara, H.; Tagawa, S. *J. Am. Chem. Soc.* **2004**, *126*, 3521−3528.
(41) Balan, B.; Vijayakumar, C.; Saeki, A.; Koizumi, Y.; Tsuji, M.; Seki, S. *Polym. Chem.* **2013**, *4*, 2293.
(42) Bracco, S.; Comotti, A.; Ferretti, L.; Sozzani, P. *J. Am. Chem. Soc.* **2011**, *133*, 8982−8994.
(43) Hohwy, M.; Jakobsen, H. J.; Edén, M.; Levitt, M. H.; Nielsen, N. C. *J. Chem. Phys.* **1998**, *108*, 2686−2694.
(44) Madhu, P. K.; Vinogradov, E.; Vega, S. *Chem. Phys. Lett.* **2004**, *394*, 423−428.
(45) Brown, S. P. *Solid State Nucl. Magn. Reson.* **2012**, *41*, 1−27.
(46) Becker, J.; Comotti, A.; Simonutti, R.; Sozzani, P.; Saalwächter, K. *J. Phys. Chem. B* **2005**, *109*, 23285−23294.
(47) Bukalov, S. S.; Leites, L. A.; Magdanurov, G. I.; West, R. *J. Organomet. Chem.* **2003**, *685*, 51−59.
(48) Bukalov, S. S.; Zubavichus, Y. V.; Leites, L. A.; Koe, J. R.; West, R. *Polymer* **2009**, *50*, 4845−4851.
(49) Okumura, H.; Kawaguchi, Y.; Harada, A. *Macromolecules* **2003**, *36*, 6422−6429.
(50) Bovey, F. A.; Schilling, F. C. In *Solid State NMR of Polymers*; Plenum Press: New York, 1991; pp 295−304.
(51) Sozzani, P.; Comotti, A.; Bracco, S.; Simonutti, R. *Chem. Commun.* **2004**, 768−769.
(52) Comotti, A.; Simonutti, R.; Catel, G.; Sozzani, P. *Chem. Mater.* **1999**, *11*, 1476−1483.
(53) Sozzani, P.; Bovey, F. A.; Schilling, F. C. *Macromolecules* **1991**, *24*, 6764−6768.
(54) Sozzani, P.; Galimberti, M.; Balbontin, G. *Makromol. Chem., Rapid Commun.* **1992**, *13*, 305−310.
(55) Krebs, F. C.; Jørgensen, M. *Macromolecules* **2003**, *36*, 4374−4384.
(56) Saeki, A.; Seki, A.; Koizumi, Y.; Sunagawa, T.; Ushida, K.; Tagawa, S. *J. Phys. Chem. B* **2005**, *109*, 10015−10019.
(57) Balan, B.; Vijayakumar, C.; Saeki, A.; Koizumi, Y.; Tsuji, M.; Seki, S. *Polym. Chem.* **2013**, *4*, 2293−2303.
(58) Hoofman, R. J. O. M.; De Haas, M. P.; Siebbeles, L. D. A.; Warman, J. M. *Nature* **1998**, *392*, 54−56.
(59) Fujino, M. *Chem. Phys. Lett.* **1987**, *136*, 451−453.
(60) Van der Laan, G. P.; De Haas, M. P.; Hummel, A.; Frey, H.; Möller, M. *J. Phys. Chem.* **1996**, *100*, 5470−5480.
(61) Naito, N.; Nakamura, M.; Terao, K.; Kawabe, T.; Fujiki, M. *Macromolecules* **2010**, *43*, 7919−7923.
(62) Ma, N.; Yu, Y.; Sun, A.; Huang, S. *J. Lumin.* **2007**, *126*, 827−832.
(63) Ban, H.; Sukegawa, K. *J. Appl. Polym. Sci.* **1987**, *33*, 2787−2793.
(64) Watanabe, A.; Matsuda, M. *Macromolecules* **1992**, *25*, 484−488.

DOI: 10.1021/jacs.5b02215
J. Am. Chem. Soc. 2015, 137, 5231−5238